

Article

Single- to Triple-Wall WS₂ Nanotubes Obtained by High-Power Plasma Ablation of WS₂ Multiwall Nanotubes

Volker Brüser ^{1,†}, Ronit Popovitz-Biro ^{2,†}, Ana Albu-Yaron ^{3,†}, Tommy Lorenz ^{4,†},
Gotthard Seifert ^{4,†}, Reshef Tenne ^{3,†} and Alla Zak ^{5,†,*}

¹ Leibnitz Institute for Plasma Science and Technology (INP), Felix-Hausdorff-Straße 2, 17489 Greifswald, Germany; E-Mail: brueser@inp-greifswald.de

² Department of Chemical Research Support, Weizmann Institute of Science, P.O. Box 26, Rehovot 76100, Israel; E-Mail: Ronit.Popovitz@weizmann.ac.il

³ Department of Materials and Interfaces, Weizmann Institute of Science, P.O. Box 26, Rehovot 76100, Israel; E-Mails: ana.albu-yaron@weizmann.ac.il (A.A.-Y.); reshef.tenne@weizmann.ac.il (R.T.)

⁴ Physikalische Chemie, Technische Universität Dresden, Bergstrasse, 66b, 01062 Dresden, Germany; E-Mails: Tommy.Lorenz@chemie.tu-dresden.de (T.L.)
gotthard.seifert@chemie.tu-dresden.de (G.S.)

⁵ Faculty of Science, Holon Institute of Technology, P.O. Box 305, Holon 58102, Israel

† These authors contributed equally to this work.

* Author to whom correspondence should be addressed: E-Mail: alzak@hit.ac.il;
Tel.: +972-3-502-6802; Fax: 972-3-502-6619.

Received: 15 March 2014; in revised form: 21 April 2014 / Accepted: 21 April 2014 /

Published: 29 April 2014

Abstract: The synthesis of inorganic nanotubes (INT) from layered compounds of a small size (<10 nm in diameter) and number of layers (<4) is not a trivial task. Calculations based on density functional tight-binding theory (DFTB) predict that under highly exergonic conditions, the reaction could be driven into a “window” of (meta-) stability, where 1–3-layer nanotubes will be formed. Indeed, in this study, single- to triple-wall WS₂ nanotubes with a diameter of 3–7 nm and a length of 20–100 nm were produced by high-power plasma irradiation of multiwall WS₂ nanotubes. As target materials, plane crystals (2H), quasi spherical nanoparticles (IF) and multiwall, 20–30 layers, WS₂ nanotubes were assessed. Surprisingly, only INT-WS₂ treated by plasma resulted in very small, and of a few layers, “daughter” nanotubules. The daughter nanotubes occur mostly attached to the outer surface of the predecessor, *i.e.*, the multiwall “mother” nanotubes.

They appear having either a common growth axis with the multiwall nanotube or tilted by approximately 30° or 60° with respect to its axis. This suggests that the daughter nanotubes are generated by exfoliation along specific crystallographic directions. A growth mechanism for the daughter nanotubes is proposed. High resolution transmission and scanning electron microscopy (HRTEM/HRSEM) analyses revealed the distinctive nanoscale structures and helped elucidating their growth mechanism.

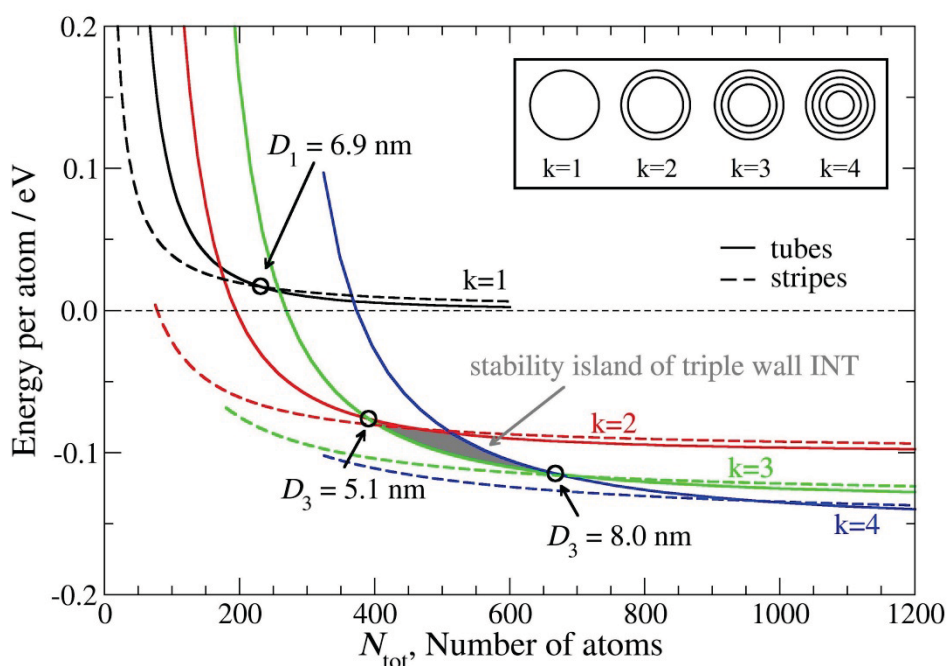
Keywords: single-wall inorganic nanotubes; growth mechanism; multiwall inorganic nanotubes; WS₂; high power plasma ablation; window of stability

1. Introduction

Multiwall inorganic nanotubes of WS₂ (INT-WS₂) were discovered in 1992 [1], and the route for their scaled-up synthesis was developed in 2009 [2]. Together with BN [3] and MoS₂ [4,5], they probably constitute the most investigated kind of inorganic nanotubes from layered compounds. The crystalline and electronic structure of INT has been studied in great detail [6–8]. In particular, calculations have shown that multiwall WS₂ (MoS₂) nanotubes become more stable than the respective nanosheets at a threshold outer diameter of about 15 to 20 nm and being made up of at least 5–10 layers [9]. Indeed, many of the high-temperature (above 700 °C) synthetic strategies ended up in multiwall nanotubes exhibiting a high-crystalline order, which agree quite well with the predicted sizes [2,10,11].

Nonetheless, these conditions are not sufficiently exergonic to drive the reaction into windows of (meta-) stability far enough from equilibrium, where 1–3-layer nanotubes could be formed. It was shown in the past that reactions carried out under highly exergonic conditions, like laser ablation [12], for example, can yield closed-cage MoS₂ nanoparticles having a small size and number of layers. Calculations based on density functional tight-binding theory (DFTB) [9] (see Figure 1) present the energy-per-atom of nanotubes as a function of the number of atoms in the unit length (unit cell), N_{tot} , and for different number of layers ($k = 1-4$). They are compared with nanostripes (nanoribbons) of the same number of atoms. For the sake of simplicity, the calculations were carried out for MoS₂, which is structurally analogous to WS₂. It is noticed that the energy-per-atom increases with a decreasing number of atoms for both the nanostripes and the nanotubes, but for different reasons. The energy-per-atom for the nanostripes increases, due to edge effects, *i.e.*, the abundance of rim atoms with dangling bonds. On the other hand, the nanotubes become less stable at a smaller radius of curvature, due to the increasing elastic energy of folding. In addition, the folding energy increases more steeply for the nanotubes than the energy of the nanoribbons as the number of atoms shrinks. Consequently, smaller diameter nanotubes become less stable than the straight nanostripes to the left of the cross-over point (stability threshold) of the two curves. While the cross-over point itself moves to the left as the number of layers decreases, the corresponding threshold energy-per-atom rapidly increases (becomes less negative), particularly for nanotubes with three layers and below. It is therefore clear that the generation of nanotubes of a small size and number of layers ($k < 4$) requires highly exergonic conditions, which is the subject of the present work.

Figure 1. The calculated energy-per-atom for MoS₂ nanotubes and nanostripes with 1–4 walls as a function of the number of atoms in the tube unit cell, N_{tot} .



Interestingly, in the range of $\sim 390 < N_{\text{tot}} < 670$, which corresponds to nanotubes with outer diameters of $5.1 \text{ nm} < D_3 < 8.0 \text{ nm}$, the triple layer nanotubes are more stable than nanotubes with $k = 2$ and $k = 4$ (see Figure 1). The diameter (D_k) represents here the outer diameters of the nanotubes with k shells. This theoretical prediction is in agreement with experimental results presented in this work: the majority of the daughter nanotubes were triple-walled. Note that nanotubes with the same (outer) diameters, but different number of shells, have consequently a different (total) number of atoms. Thus, a single-wall tube with a larger diameter may have less atoms than triple-walled tubes of a smaller diameter.

A similar situation has been encountered with the stability window of MoS₂ nanotetrahedra and nanooctahedra consisting of 2–4 layers. These nanostructures were proposed first in [13,14] and realized in [15,16]. Indeed, MoS₂ nanooctahedra/nanotetrahedra were obtained by rapid quenching of laser- [15–18] or solar- [19] ablated MoS₂ soot or by an arc-discharge process [20]. It can, therefore, be concluded that highly exergonic reaction conditions and rapid quenching of the nanoclusters can access (meta-) stability windows, which favor new nanotubes that are not reachable by the conventional thermally-driven synthesis at < 1000 °C.

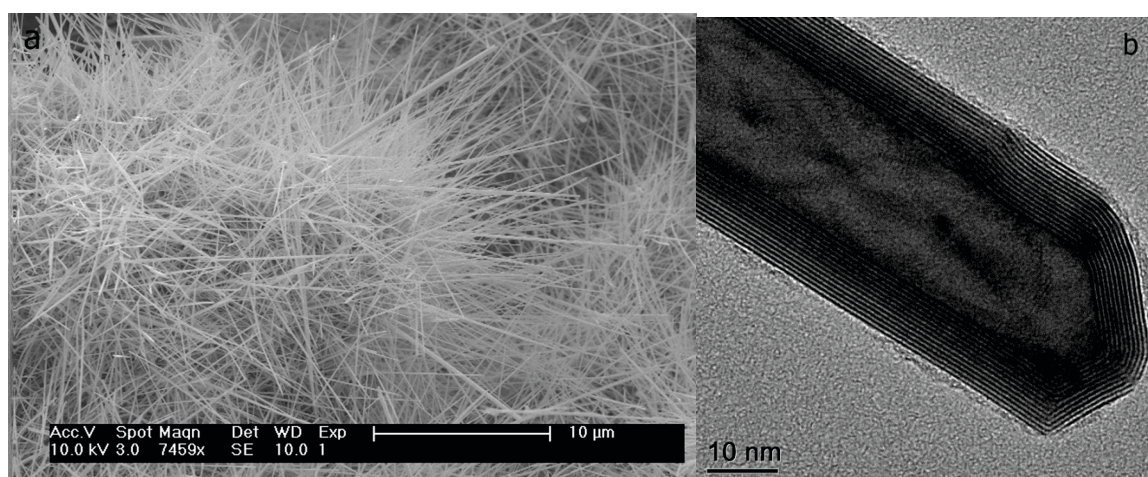
2. Results and Discussion

In the present work, 1–3-layer WS₂ nanotubes with a diameter of 3–7 nm and a length of 20–100 nm were produced by applying inductively coupled radio-frequency plasma irradiation on multiwall INT-WS₂.

2.1. Scanning and Transmission Electron Microscopy Analysis

Typical scanning and transmission electron microscopy images of a pristine (untreated) multiwall WS₂ (“mother”) nanotube are presented in Figure 2a,b, respectively. The majority of the predecessor INT was 5–20 microns in length and 30–120 nm in diameter.

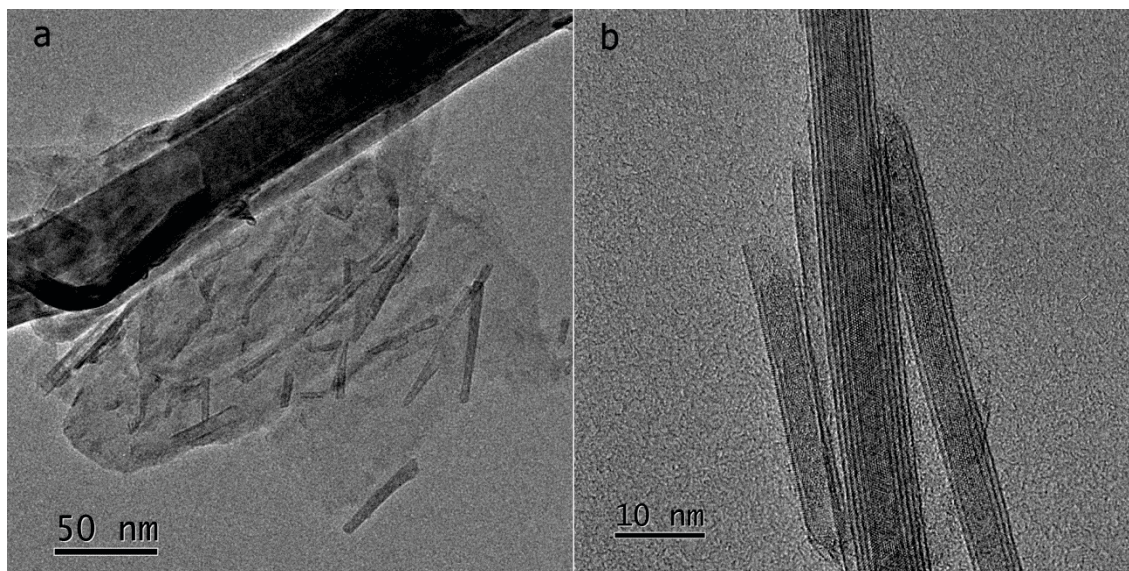
Figure 2. (a) SEM and (b) TEM micrograph of a pristine multiwall WS₂ nanotube.



The HRTEM images in Figure 3a,b display the range of daughter nanotubes obtained by plasma-treating of the multiwall WS₂ nanotubes at 600 W for 40 min: tiny daughter nanotubes adjacent to the outer surface (Figure 3a) of the mother nanotube and a few isolated daughter nanotubes (Figure 3b). The amount of such daughter nanotubes increased with the treatment time from 10 to 40 min at 400 W plasma power. The extension of the plasma treatment time to 80 min did not reveal any additional improvement; however, the increase of plasma power from 400 to 600 W resulted in a sharp increase in the amount of the daughter nanotubes.

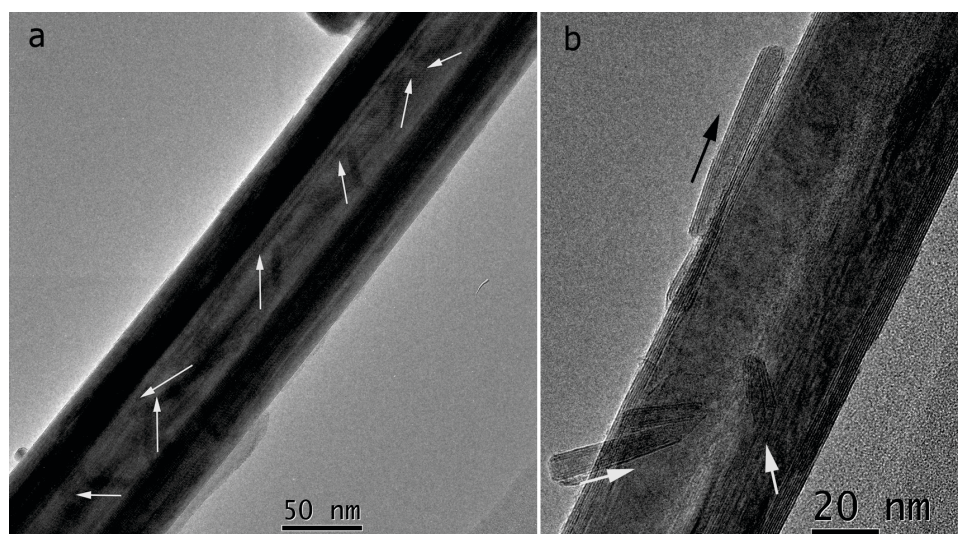
At 600 W and 40 min of treatment, a rough statistical estimate shows that daughter nanotubes were attached to about 80% of the plasma treated multiwall nanotubes. In comparison, only 10–20% of the multiwall WS₂ nanotubes were covered with daughter nanotubes by a 400-W plasma treatment. Some nanostructures could be better described as nanoscrolls. However, the majority of the daughter nanostructures are nanotubes, having at least one perfectly closed layer. Future work will be focused on devising this technique to increase the yield of a single- to a few-layer nanotubes of WS₂ or other INT, as well. Indeed, by irradiating MoS₂ powder with a focused solar beam, single-wall MoS₂ was rarely observed in the processed powder [21], which confirms that highly exergonic conditions produced by focused solar (laser) ablation may lead to the production of single-wall nanotubes of this kind.

Figure 3. TEM images of daughter WS₂ nanotubes obtained by plasma ablation of multiwall inorganic nanotube (INT)-WS₂ at 600 W for 40 min: (a) A large number of daughter nanotubes next to a treated multiwall nanotube; (b) A group of daughter nanotubes isolated from plasma-treated multiwall WS₂ nanotubes by sonication.



Moreover, many daughter nanotubes were found attached and being tilted at *ca.* 30 or 60° with respect to the mother nanotube axis (see the white arrows in Figure 4a,b). However, some daughter nanotubes were found to be attached, having a common growth axis with the multiwall nanotube (see the black arrow in Figure 4b).

Figure 4. (a) TEM images of the daughter nanotubes tethered to the surface and tilted at approximately 30 or 60° with respect to the mother nanotube growth axis (white arrows); (b) TEM image of a daughter nanotube with growth axis parallel to the mother nanotube (black arrows).

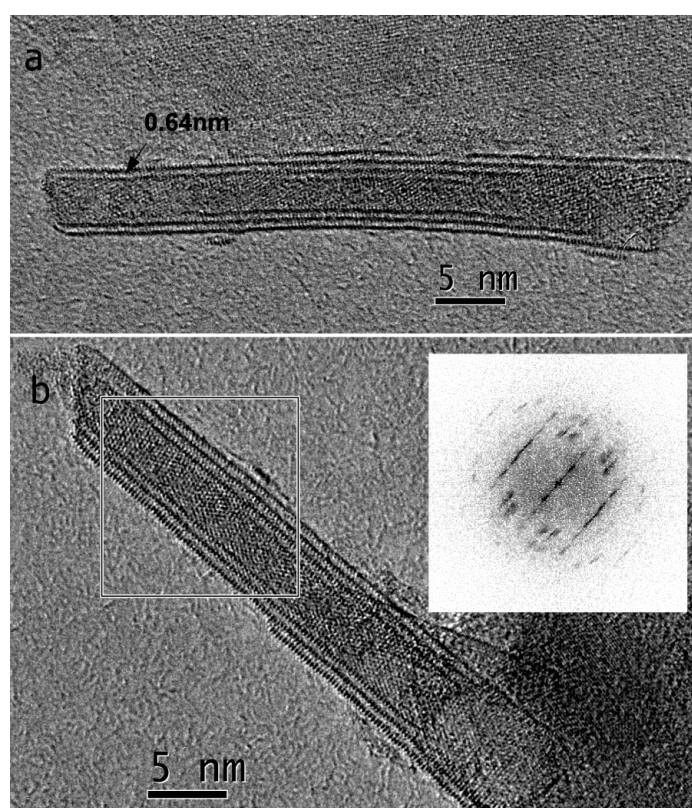


These observations suggest that the small nanotubes were exfoliated by unzipping the outer walls of the mother nanotubes along specific crystallographic directions. In addition to nanotubes/nanoscrolls, a

few layers-thick WS₂ nanoplatelets of typical sizes in the range of the nanotubes' length, *i.e.*, 50–100 nm, were also observed.

In an attempt to separate the daughter nanotubes from the mother nanotubes, the plasma-ablated WS₂ nanotube powder was ultrasonically treated in ethanol for 10 min. The high-resolution TEM (HRTEM) images in Figure 5 (see also Figure 3b) clearly depict the daughter nanotubes being more easily observed after detachment from the predecessor nanotubes.

Figure 5. (a) HRTEM images of a two–three-layer nanotube with a non-uniform diameter after detachment from the large WS₂ multiwall nanotube; (b) Another three-layer daughter nanotube after detachment. The Fourier (FFT) analysis (see the inset) of the area framed by the square shows that the nanotube is chiral with a helical angle of six degrees.

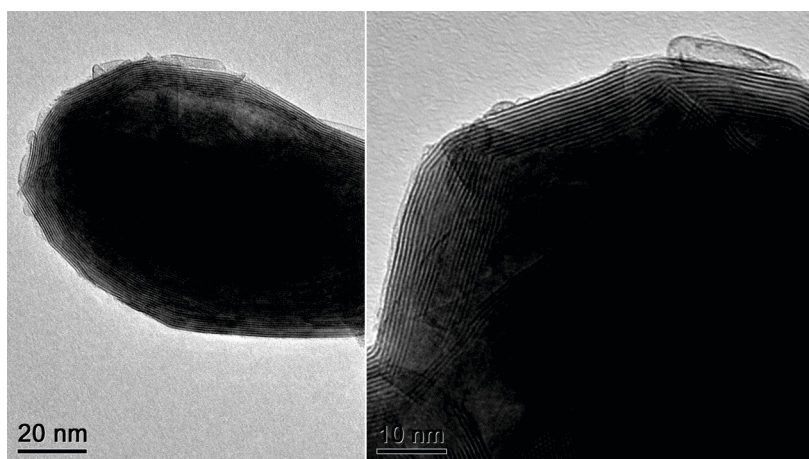


Rough statistical analysis revealed that the interlayer distance in most daughter nanotubes varied between 6.3–6.5 Å (see Figure 5a), which is larger than the interlayer spacing of 2H-WS₂ (6.23 Å/2-Theta = 14.32°) and multiwall nanotubes (6.31 Å/2-Theta = 14.13°) [2]. This observation suggests that the daughter nanotubes were not fully relaxed during the growth process and that the annealing of the sample could possibly lead to further structural relaxation. The Fourier (FFT) analysis (see the inset in Figure 5b) of the area framed by the square shows that the nanotube is chiral with a helical angle of six degrees. Once daughter nanotubes are observed in larger yields, techniques like ultracentrifugation could be used to separate them according to the number of layers and the length.

Energy dispersive X-ray analysis (EDS) within the TEM (not shown) confirmed that the nanotubes are made solely of tungsten and sulfur. Negligible traces of oxygen were found, which could be mainly attributed to surface impurities.

In a separate series of experiments, several powders of different microcrystalline layered materials, including 2H-WS₂, 2H-MoS₂ and 2H-NbS₂, and also the respective diselenides, received a similar plasma treatment. No daughter nanotubes were found in these treated samples, whatsoever. A few layers-thick WS₂ nanoplatelets with typical sizes in the range of the nanotubes (50–100 nm) were nevertheless abundant in plasma-treated 2H-WS₂ powder. Furthermore, the NbSe₂ powder turned out to be unstable under the plasma treatment conditions. Plasma treatment (400 W) of fullerene-like WS₂ nanoparticles with hollow cage structure (inorganic fullerene-like (IF-WS₂) nanoparticles) resulted in a few layers exfoliation and a few small-sized (“daughter”) fullerene-like nanoparticles or nanotubes (see Figure 6). The daughter IF-WS₂ nanoparticles are reminiscent of the arc-discharge produced IF-MoS₂ nanoparticles [20]. In concluding this large series of experiments, it is possible to state that only plasma irradiation of multiwall WS₂ nanotubes yielded daughter nanotubes in a reproducible fashion.

Figure 6. TEM image of the attached daughter single wall fullerene-like nanoparticles generated by plasma treatment of multiwall fullerene-like WS₂ nanoparticles.



Single-wall carbon nanotubes can be obtained in large quantities, e.g., via the arc-discharge technique [22]. Given the interlayer distance of 3.4 Å in graphite, the monoatomic graphene plane can be closed into nanotubes of a diameter smaller than 0.5 nm [23,24]. On the other hand, the WS₂ (MoS₂) layer consists of six-fold bonded tungsten (molybdenum) atoms sandwiched between two sub-layers of three-fold bonded sulfur atoms. This makes the WS₂ layers pretty rigid, with interlayer spacing of 6.23 Å; it is no wonder that the elastic energy for WS₂ (MoS₂) nanotube formation is appreciably larger than that of graphitic carbon. If one takes the elastic energy threshold for folding to be 0.05 eV/atom, the calculated diameter of a single-wall carbon nanotube is between one and 1.2 nm [25], and that of a single-wall MoS₂ should be 6.2 nm [9,26]. Therefore, the diameters of the daughter WS₂ nanotubes observed in the current series of experiments reconcile very well with the previous calculations.

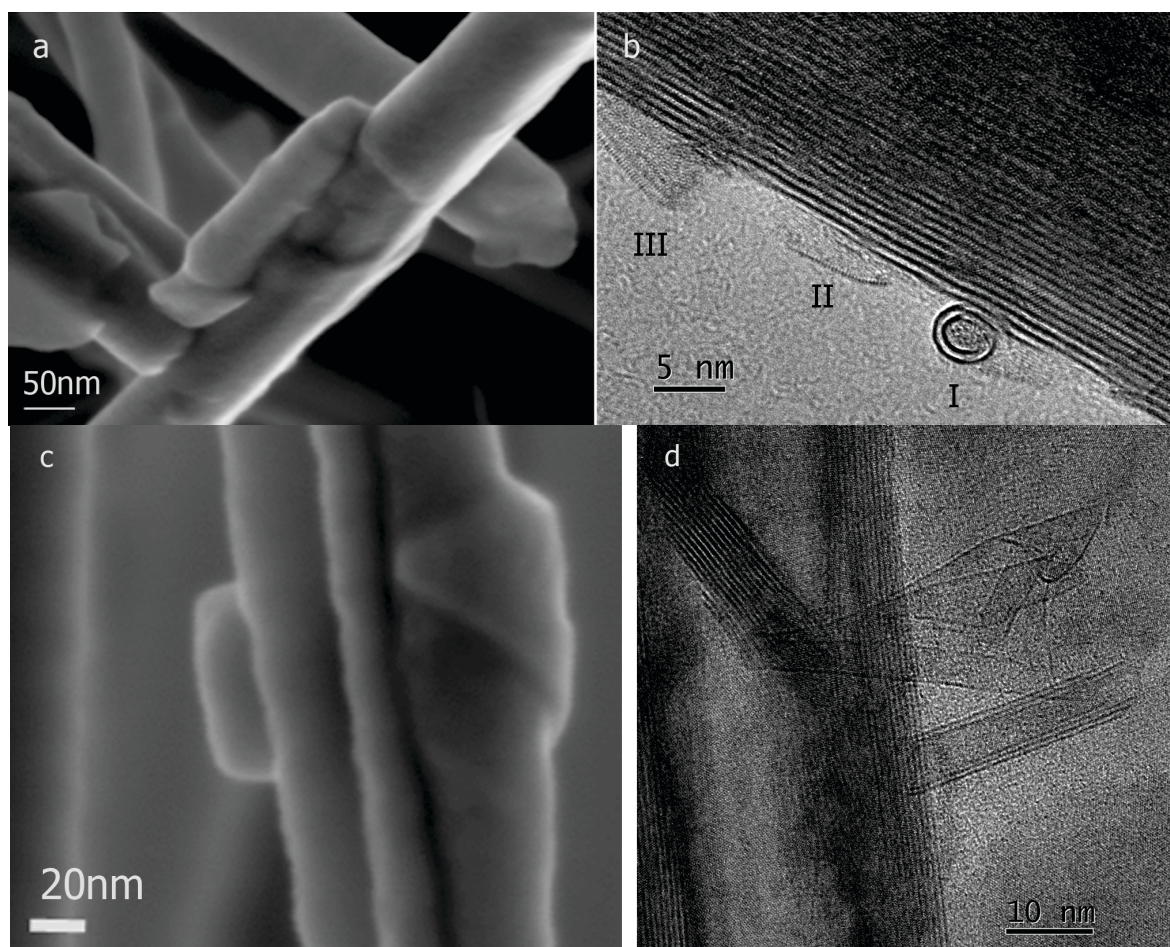
2.2. Growth Mechanism

It is hypothesized that the formation of the daughter nanotube occurs through a strong interaction of the highly energetic plasma, used in this work, with a point or line defect on the outer surface of the mother nanotube, leading to rapid unzipping and exfoliation of 1–3 layers-thick WS₂ fragments. One

way for the exfoliated nanosheets to release the large elastic strain and fold into a nanotube is through an “inverted umbrella” reaction, which is the manifestation of the “Walden inversion” typical of a nucleophilic attack of a stereoisomer by an electron-rich moiety [27].

In an effort to understand the mechanism of formation of these daughter nanotubes, additional HRSEM analysis of the plasma-treated nanotubes was undertaken. The HRSEM in Figure 7a reveals a reversely revolved nanoscroll of ~20 nm in diameter attached to the surface of the mother nanotube. Furthermore, a clearly observed step defect or dark contrast on the mother nanotube beneath the daughter nanoscroll is reminiscent of the exfoliation process of the WS₂ patch. Unfortunately, the resolution of the SEM did not permit viewing the smaller (3–7 nm) daughter nanotubes.

Figure 7. (a) HRSEM micrograph of a daughter nanoscroll attached to a large nanotube; (b) (I) HRTEM of a two-layer daughter nanoscroll viewed head-on along its axis and attached to a large multiwall nanotube; (II) an initial scrolling stage of an exfoliated single layer and three (III) layers before the formation of the nanotube; (c) HRSEM image of a daughter nanotube attached to a mother INT; and (d) HRTEM images revealing the folding of WS₂ nanosheets to form a daughter nanotube.

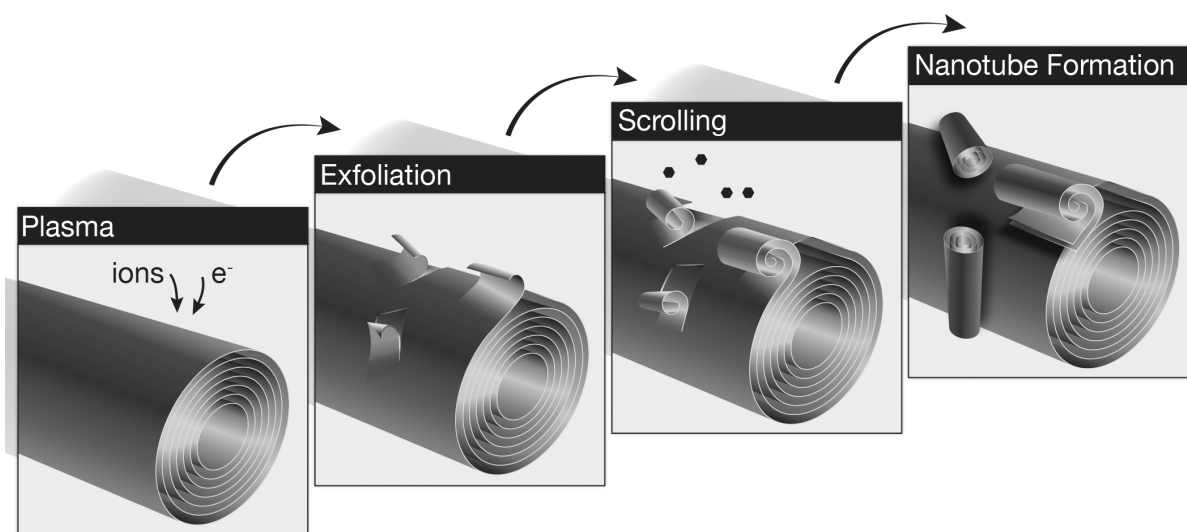


Nonetheless, this analysis suggests very strongly that the elastic strain of the exfoliated WS₂ sheet produces oppositely revolved daughter nanotubes. Moreover, at better resolution, the HRTEM image in Figure 7b depicts a two-layer daughter nanoscroll viewed head-on along its axis marked by “I”. Furthermore, an initial scrolling stage of an exfoliated single layer (“II”) and three layers (“III”) before

the formation of the nanotube was also observed. In addition, Figure 7c,d shows an HRSEM image of a daughter nanotube attached to a mother nanotube and HRTEM images of a WS_2 nanosheet in the process of folding to form a daughter nanotube.

A schematic model for the growth mechanism of the daughter nanotubes is depicted in Figure 8. This growth mechanism proposes that the fragments of the outermost (1–3) layers of the predecessor nanotubes were unzipped by the plasma treatment, exfoliated and folded into daughter nanotubes. The large excitation energies of the plasma together with the mechanical strain lead to a nanoscopic “Walden-type inversion” [27]. The reactive edges of the inverted layers induce further folding into daughter nanotubes with a smaller radius of curvature than the predecessor (mother) multiwall WS_2 nanotube. Detachment of the 1–3 layers from the mother nanotube may also be followed by rotation and inclination, in this case, the axes of the mother and daughter nanotubes do not necessarily coincide or form a specific angle between them. In other cases the rapid quenching of the excess energy of the nanosheets does not permit them to fully close, which leads to nanoscrolls or to a nanotube with one closed wall and the others remaining unclosed. Nanoscrolls may also occur due to steric hindrance, where the plasma-induced exfoliated nanosheets released their energy without being able to undergo timely inversion.

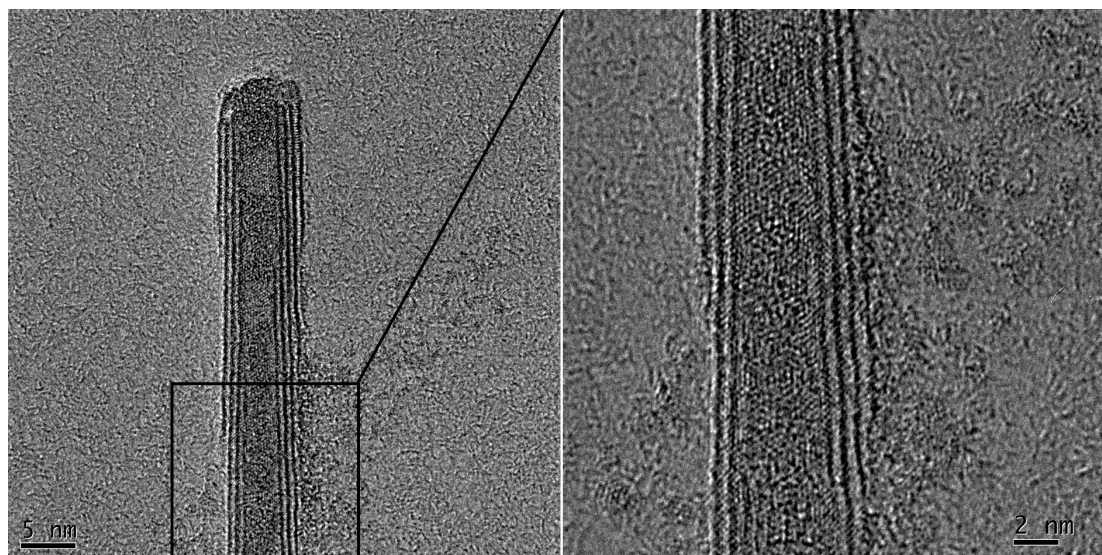
Figure 8. Schematics of the proposed growth mechanism of the daughter nanotubes by plasma treatment of the multiwall mother nanotubes.



In a few cases, WS_x nanoclusters were observed adjacent to the daughter nanotubes (see Figure 9). These non-stoichiometric nanoclusters could be obtained by the condensation of tungsten and sulfur atoms or WS_2 molecules from the vapor phase. In turn, the condensation of clusters onto the tube edges could lead to further elongation or even the growth of an extra layer on the daughter nanotube surface. Another plausible event is the condensation of the vapors into separate nanosheets, which, upon quenching, form isolated nanotubes.

The proposed mechanism is consistent with the data presented in this work. In order to shed light on the detailed growth mechanism of the (daughter) nanotubes and to control their length, diameter and the number of layers, future experiments will focus on the variation of the plasma treatment process, including the substrate temperature, pressure in the chamber, *etc.*

Figure 9. TEM images of nanoclusters surrounding daughter nanotubes. Presumably, the clusters were generated by the condensation of tungsten and sulfur atoms or WS₂ molecular clusters from the vapor phase created by the plasma treatment of the multiwall WS₂ nanotubes.



Since highly excited clusters of WS₂ (MoS₂) can be formed using arc-discharge and a variety of other techniques, high-power plasma ablation would possibly allow synthesizing a few-wall nanotubes under controlled conditions in higher yields.

3. Experimental Section

3.1. Plasma Treatment

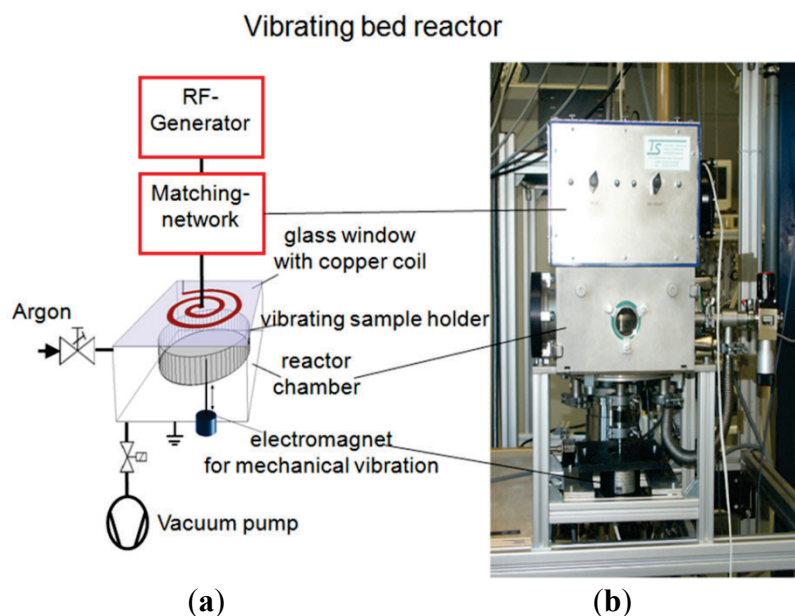
The schematic drawing and photograph of the experimental set-up for the inductively coupled radio-frequency plasma irradiation (27.12 MHz) [28] of the multiwall WS₂ nanotubes is depicted in Figure 10.

In these experiments, non-thermal plasma with electrons, atoms and ions, having different temperatures each, was used to irradiate powders of multiwall WS₂ nanotubes (INT-WS₂), inorganic fullerene-like (IF) quasi spherical nanoparticles and different transition metal dichalcogenides microcrystalline 2H-platelets. A plasma power in the range of 400–600 W was applied for 5, 10, 20, 40 and 80 min. The electron temperature in these experiments was in the range of 1.7×10^4 – 2.3×10^4 °K (1.5–2 eV), and the electron density was in the range of $\sim 10^{12}/\text{cm}^3$ [29].

The argon gas pressure was 10 Pa, and the flow speed of the Ar gas was 30–35 cm³/s, while the base pressure before the Ar gas was 10^{-4} Pa. The temperature of the neutral Ar atoms and Ar⁺ ions is approximately two orders of magnitude smaller than that of the electrons. The plasma energy impact on the substrate surfaces was 2.3 W/cm² at 400 W and 3.1 W/cm² at 600 W [30]. The plasma parameters, pressure and energy impact were constant over the treatment time. The temperature of the substrate increased with time and depended on the heat conductivity and the quality of the thermal contact between the powder and the susceptor. The nanoparticles temperature was different from that of the gas. It was influenced by a number of factors, including the electron and ion bombardment,

electron-ion recombination, reaction enthalpy from the chemical surface reaction, energy loss by heat radiation and conduction. The temperature of the nanotubes could be estimated to be in the range of a few hundred degrees centigrade [31].

Figure 10. (a) Schematic representation and (b) Photograph of the experimental set-up for the plasma treatment of the multiwall WS₂ nanotubes.



3.2. Electron Microscopy

The resulting samples were examined by transmission electron microscopy (TEM) (Philips CM120 operating at 120 kV, equipped with an energy dispersive X-ray spectroscopy (EDS) detector (EDAX Phoenix Microanalyzer) for chemical analysis). High-resolution TEM (HRTEM) (FEI Technai F30-UT, with a field-emission gun operating at 300 kV) and scanning transmission electron microscopy (STEM) (FEI Technai F20 operating at 200 kV equipped with a high-angle annular dark field (HAADF) detector and EDS detector (EDAX-Phoenix Microanalyzer)) were also used. Complementary information was obtained by high-resolution scanning electron microscopy (HRSEM) (Zeiss Ultra model V55 and LEO model Supra 55VP equipped with an EDS detector (Oxford model INCA) and backscattering electron (BSE) detector).

4. Conclusions

In conclusion, WS₂ nanotubes of 1–3 layers (“daughter nanotubes”), 20–100 nm-long and with diameters varying between 3–7 nm, were obtained by plasma treatment of multiwall nanotubes in inert atmosphere. The proposed growth mechanism of the daughter nanotubes involves the strong interaction of the plasma with point or line defects, causing unzipping and exfoliation of the outermost layers of the multiwall nanotube, the release of the elastic strain, followed by scrolling and closure into small nanoscrolls or nanotubes. Sublimation of W and S atoms, WS₂ molecules and cluster formation could serve as an additional building material for daughter tube formation and extension. These few-layered WS₂ nanotubes represent a locally stable, highly excited state of this solid. Being of such

small dimensions, they should reveal a quantum confinement effect, as well as new optical, electrical and mechanical properties. Furthermore, these nanotubes can be suspended in different solvents and could possibly be of particular interest, e.g., for drug delivery.

Acknowledgments

We gratefully acknowledge Gal Radovski for assisting with the HRSEM microscopy analysis. We gratefully acknowledge the support of the ERC project *INTIF* 226639, ITN *MoWSeS* 317451, the Israel Science Foundation, the COST action *COINAPO* MP0902, the FTA project of the Isr. Natl. NanoInitiative; the G.M.J. Schmidt Minerva Center for supramolecular chemistry; the Harold Perlman and the Irving and Azelle Waltcher Foundations, and the Irving and Cherna Moskowitz Center for Nano and Bio-Nano Imaging. R.T. is the Drake Family Chair in Nanotechnology and director of the Helen and Martin Kimmel Center for Nanoscale Science.

Author Contributions

V.B.: Plasma treatment; R.P.-B.: TEM analyses and discussion of the results; A.A.-Y.: TEM analysis and discussion of the results; T.L.: Theoretical calculations; G.S.: Theoretical calculations; R.T.: Analysis of the nanotubes, discussion and the dissemination of the results; A.Z.: Synthesis of inorganic multiwall WS₂ nanotubes, TEM/SEM analyses, discussion of the plasma experiment, discussion the dissemination of the results.

Conflicts of Interests

The authors declare no conflict of interests.

References

1. Tenne, R.; Margulis, L.; Genut, M.; Hodes, G. Polyhedral and cylindrical structures of tungsten disulphide. *Nature* **1992**, *360*, 444–446.
2. Zak, A.; Sallacan-Ecker, L.; Margolin, A.; Genut, M.; Tenne, R. Insight into the growth mechanism of WS₂ nanotubes in the scaled-up fluidized-bed reactor. *Nano* **2009**, *4*, 91–98.
3. Chopra, N.G.; Luyken, J.; Cherry, K.; Crespi, V.H.; Cohen, M.L.; Louie, S.G.; Zettl, A. Boron Nitride Nanotubes. *Science* **1995**, *269*, 966–967.
4. Feldman, Y.; Wasserman, E.; Srolovitz, D.J.; Tenne, R. High-rate, gas-phase growth of MoS₂ nested inorganic fullerenes and nanotubes. *Science* **1995**, *267*, 222–225.
5. Remskar, M.; Skraba, Z.; Cleton, F.; Sanjines, R.; Levy, F. MoS₂ as microtubes. *Appl. Phys. Lett.* **1996**, *69*, 351–353.
6. Rubio, A.; Corkill, J.F.; Cohen, M.L. Theory of graphitic boron nitride nanotubes. *Phys. Rev. B* **1994**, *49*, 5081–5084.
7. Seifert, G.; Terrones, H.; Terrones, M.; Jungnickel, G.; Frauenheim, T. Structure and electronic properties of MoS₂ nanotubes. *Phys. Rev. Lett.* **2000**, *85*, 146–149.

8. Linnolahti, M.; Pakkanen, T.A. Quantum chemical treatment of large nanotubes via use of line group symmetry: Structural preferences of magnesium dichloride nanotubes. *J. Phys. Chem. B* **2006**, *110*, 4675–4678.
9. Seifert, G.; Köhler, T.; Tenne, R. Stability of metal chalcogenide nanotubes. *J. Phys. Chem. B* **2002**, *106*, 2497–2501.
10. Therese, H.A.; Li, J.; Kolb, U.; Tremel, W. Facile large scale synthesis of WS₂ nanotubes from WO₃ nanorods prepared by a hydrothermal route. *Solid State Sci.* **2005**, *7*, 67–72.
11. Li, Y.D.; Li, X.L.; He, R.R.; Zhu, J.; Deng, Z.X. Artificial lamellar mesostructures to WS₂ nanotubes. *J. Am. Chem. Soc.* **2002**, *124*, 1411–1416.
12. Sen, R.; Govindaraj, A.; Suenaga, K.; Suzuki, S.; Kataura, H.; Iijima, S.; Achiba, Y. Encapsulated and hollow closed-cage structures of WS₂ and MoS₂ prepared by laser ablation at 450–1050 °C. *Chem. Phys. Lett.* **2001**, *340*, 242–248.
13. Margulis, L.; Salitra, G.; Tenne, R.; Talianker, M. Nested fullerene-like structures. *Nature* **1993**, *365*, 113–114.
14. Tenne, R. Doped and Heteroatom-Containing Fullerene-like Structures and Nanotubes. *Adv. Mater.* **1995**, *7*, 965–995.
15. Singh, D.M.D.J.; Pradeep, T.; Bhattacharjee, J.; Waghmare, U.V. Novel cage clusters of MoS(2) in the gas phase. *J. Phys. Chem. A* **2005**, *109*, 7339–7342.
16. Parilla, P.A.; Dillon, A.C.; Jones, K.M.; Riker, G.; Schulz, D.L.; Ginley, D.S.; Heben, M.J. The first true inorganic fullerenes? *Nature* **1999**, *397*, 114.
17. Enyashin, A.N.; Gemming, S.; Bar-Sadan, M.; Popovitz-Biro, R.; Hong, S.Y.; Prior, Y.; Tenne, R.; Seifert, G. Structure and stability of molybdenum sulfide fullerenes. *Angew. Chem. Int. Ed.* **2007**, *46*, 623–627.
18. Enyashin, A.N.; Bar-Sadan, M.; Sloan, J.; Houben, L.; Seifert, G. Nanoseashells and nanooctahedra of MoS₂: Routes to inorganic fullerenes. *Chem. Mater.* **2009**, *21*, 5627–5636.
19. Albu-Yaron, A.; Levy, M.; Tenne, R.; Popovitz-Biro, R.; Weidenbach, M.; Bar-Sadan, M.; Houben, L.; Enyashin, A.N.; Seifert, G.; Feuermann, D.; *et al.* MoS₂ hybrid nanostructures: from octahedral to quasi-spherical shells within individual nanoparticles. *Angew. Chem. Int. Ed.* **2011**, *123*, 1850–1854.
20. Alexandrou, I.; Sano, N.; Burrows, A.; Meyer, R.R.; Wang, H.; Kirkland, A.I.; Kiely, C.J.; Amaratunga, G.A.J. Structural investigation of MoS₂ core-shell nanoparticles formed by an arc discharge in water. *Nanotechnology* **2003**, *14*, 913–917.
21. Gordon, J.M.; Katz, E.A.; Feuermann, D.; Albu-Yaron, A.; Levy, M.; Tenne, R. Singular MoS₂, SiO₂ and Si nanostructures—synthesis by solar ablation. *J. Mater. Chem.* **2003**, *18*, 458–462.
22. Journet, C.; Maser, W.K.; Bernier, P.; Loiseau, A.; de-la Chapelle, M.L.; Lefrant, S.; Deniard, P.; Lee, R.; Fischer, J.E. Large-scale production of single-walled carbon nanotubes by the electric-arc technique. *Nature* **1997**, *388*, 756–758.
23. Qin, L.-C.; Zhao, X.; Hirahara, K.; Miyamoto, Y.; Ando, Y.; Iijima, S. Materials science: The smallest carbon nanotube. *Nature* **2000**, *408*, 50.
24. Wang, N.; Tang, Z.K.; Li, G.D.; Chen, J.S. Materials science: Single-walled 4 Å carbon nanotube arrays. *Nature* **2000**, *408*, 50–51.

25. Hernandez, E.; Goze, C.; Bernier, P.; Rubio, A. Elastic properties of C and $B_xC_yN_z$ composite nanotubes. *Phys. Rev. Lett.* **1998**, *80*, 4502–4505.
26. Lorenz, T.; Teich, D.; Joswig, J.-O.; Seifert, G. Theoretical study of the mechanical behavior of individual TiS_2 and MoS_2 nanotubes. *J. Phys. Chem. C* **2012**, *116*, 11714–11721.
27. Koshland, D.E. Stereochemistry and the mechanism of enzymatic reactions. *Biolog. Rev.* **1953**, *28*, 416–436.
28. Herrmann, I.; Brüser, V.; Fiechter, S.; Kersten, H.; Bogdanoff, P. Electrocatalysts for oxygen reduction prepared by plasma treatment of carbon-supported cobalt tetramethoxyphenylporphyrin. *J. Electrochem. Soc.* **2005**, *152*, A2179–A2185.
29. Meichsner, J.; Schmidt, M.; Schneider, R.; Wagner, H.E. *Nonthermal Plasma Chemistry and Physics*; CRC Press: Boca Raton, FL, USA, 2013; **Section 3.8.7**, pp. 120–121.
30. Savastenko, N.A.; Müller, S.; Anklam, K.; Brüser, M.; Quade, A.; Walter, C.; Brüser, V. Effect of plasma treatment on the properties of Fe-based electrocatalysts. *Surf. Coat. Technol.* **2011**, *205*, 439–442.
31. Kortshagen, U. Nonthermal plasma synthesis of semiconductor nanocrystals. *J. Phys. D Appl. Phys.* **2009**, *42*, 113001.

© 2014 by the authors; licensee MDPI, Basel, Switzerland. This article is an open access article distributed under the terms and conditions of the Creative Commons Attribution license (<http://creativecommons.org/licenses/by/3.0/>).